J. Phys.: Condens. Matter 7 (1995) 1771–1788. Printed in the UK

Molecular dynamics simulation of α- and β-cristobalite

Ian P Swainson†‡ and Martin T Dove†

† Mineral Physics Group, Department of Earth Sciences, University of Cambridge, Downing Street, Cambridge CB2 3EQ, UK

‡ Neutron and Condensed Matter Science, AECL Research, Chalk River Laboratories, Chalk River, Ontario K0J 1J0, Canada

Received 14 October 1994, in final form 28 December 1994

Abstract. A molecular dynamics simulation of the α- and β-phases of cristobalite has been performed. The simulated β-phase was found to be much more disordered than the α-phase, in agreement with evidence from many experimental techniques. The nature of the disorder was found to be dynamic, in agreement with results from many experimental techniques, but no distinct domains were detected. The results are in agreement with the rigid unit mode (RUM) model of framework structures, and recent inelastic measurements.

1. Introduction

1.1. Recent work on the structure of cristobalite and the phase transition

Cristobalite is the stable phase of SiO_2 above 1743 K at ambient pressures. It is easily quenched below this temperature and exists in a metastable state without conversion to either the tridymite or quartz forms. At ambient pressures there are two phases of cristobalite, a low-temperature tetragonal form of space group $P4_12_12$, the α-phase, and a high-temperature cubic form of space group $Fd\bar{3}m$, the β-phase. The low-temperature form is chiral and so may also be described by $P4_32_12$. The transition between these two phases occurs in the metastable temperature range ($T_{tr} \simeq 540$ K) and is strongly discontinuous. The precise transition temperature can be altered by the presence of defects like stacking faults or chemical impurities, and there is a hysteresis in the measured value of T_{tr} on heating and cooling. Furthermore, infrared spectroscopy and NMR studies have shown that the transition occurs over a range of temperatures rather than at a single transition temperature.

A number of detailed experimental studies have been carried out on the phase transition in cristobalite. Early x-ray and neutron diffraction data of the crystal structures of the α- and β-phases have recently been extended by high-resolution neutron and x-ray powder diffraction measurements [1]. When all the crystallographic results were taken together it was shown that the phase transition could be described within the framework of a simple Landau free-energy function, and, despite the large discontinuity at T_{tr}, the temperature dependence of the mean field order parameter was shown to be accurately modelled over a wide temperature range. The powder diffraction studies showed that the large spontaneous strains that accompany the phase transition—the tetragonal cell parameters a and c shrink by 3% and 5% respectively at T_{tr}—follow as the square of the order parameter. Unfortunately, the crystallographic data have not provided an unambiguous description of the structure of the β-phase. As we will describe below, there have been a number of different models

0953-8984/95/091771+18$19.50

proposed to try to reconcile the crystallographic data with crystal-chemical constraints, but all these models invoke disorder of some kind. Among the recent experiments that have been performed to shed light on this disorder are infrared and Raman spectroscopy [2], nuclear magnetic resonance [3, 4], electron diffraction [5, 6], high-temperature x-ray powder diffraction [7], and inelastic neutron scattering [8]. A detailed theoretical study of the phase transition which led to a new model for the β-phase was carried out by Hatch and Ghose [9], and more recently electronic structure calculations have been performed [10, 11]. Some experimental work has also been carried out on the related material $AlPO_4$ [4, 12, 13], and most recently the transition in this material has been examined theoretically [14].

1.2. Models of β-cristobalite

The first description of the structure of the β-phase, known as the 'ideal' model, was given by Wyckoff [15, 16]. He suggested that the silicon and oxygen atoms occupy, respectively, the special equivalent positions 8*a* and 16*c* in the space group $Fd\bar{3}m$, which are separated by the vector [1/8,1/8,1/8]. In this structure the Si–O–Si bond angle is constrained to be 180°, and the Si–O bond is only 1.54 Å in length. This is counter to the behaviour in most other silicates at ambient pressure, where the Si–O–Si bond angle is typically between 140–150° and the Si–O bond length is around 1.61 Å. To overcome this difficulty with the 'ideal' model, several disordered models have been proposed. One of the earliest was that of Nieuwenkamp [17]. In this model the oxygen atoms do not lie on well-defined positions, but the Si–O bond precesses about its average orientation so that the oxygen atoms lie on an annulus of fixed radius. An annular radius of 0.49 Å corresponds to an Si–O bond length of 1.61 Å and an Si–O–Si bond angle of 145°, which are much more realistic from a chemical viewpoint.

One of the more popular models has been the statically disordered model of Wright and Leadbetter [18]. In this model, the oxygen atoms are placed in the 96*h* sites, with partial occupancy of 1/6. In order to minimise the distortion of the SiO_4 tetrahedra, Wright and Leadbetter [18] extended their model to include short-range order, and proposed that the structure of the β-phase consists of small domains of tetragonal symmetry, space group $I\bar{4}2d$. Due to the loss of the $\bar{3}$ axis, there are six possible orientations of this cell, so that the β-phase is actually an average over domains of all orientations, and thereby the macroscopic cubic symmetry $Fd\bar{3}m$ is recovered. In each domain the Si–O bond lengths and Si–O–Si bond angles have realistic values. Some support for this model has recently been given by the electronic structure calculations of Liu *et al* [10].

More recently the model of Wright and Leadbetter [18] has been challenged using symmetry arguments by Hatch and Ghose [9]. These authors suggest that the β-phase consists of domains of symmetry of the α-phase. Their symmetry arguments show six possible orientations of the tetragonal unit cell of each of the two chiral forms of the α-phase giving twelve distinct twins. In their model, the macroscopic symmetry of the β-phase is given by averaging over all α-domain configurations. Hatch and Ghose [9] argue that the principal objection to the model of Wright and Leadbetter [18] is that the tetragonal space group proposed as the symmetry of the domains, $I\bar{4}2d$, is not a supergroup of the space group of the α-phase, $P4_12_12$.

What is not clear in either of the proposed domain models is the expected size or life time of the domains. Certainly no experimental data are available on this point. For domain models to be realistic the domains need to be large enough and to live for long enough to be recognisable as such—we presume that the lower limits are a few unit cells in size and of the order of a few phonon periods. Our own Raman and infrared spectroscopic studies [2]

and the Raman study of Bates [19] provide no evidence for the existence of recognisable domains of any sort, and indeed the spectroscopic data strongly suggest that domains do not exist, other than those formed as transient fluctuations.

We have therefore proposed a more general interpretation of the disorder in the β-phase based upon the rigid unit mode (RUM) model which was initially proposed to solve a number of problems associated with the phase transitions in quartz [20] and more recently generalized to any framework silicate by Dove *et al* [21, 22] and Giddy *et al* [23]. Because this model is central to the work presented in this paper, we describe it in some detail in a separate section below. However, we note that in this model the two domain models of Wright and Leadbetter [18] and Hatch and Ghose [9] assume an equivalent status. Both types of domains can occur within the structure at once, and low energy domain walls between domains can easily be formed. These are simply constructed as different linear combinations of the same set of RUM displacements. However, the phase space for domain formation is rather larger than the six or twelve pockets proposed by either model. Thus there are a large number of ways that the structure can accommodate realistic Si–O bond lengths and Si–O–Si bond angles without any need for significant distortions of the ideal SiO_4 tetrahedra.

1.3. Experimental evidence of disorder in β-cristobalite

We have noted that the implausibility of the 'ideal' model has led to the suggestion of disorder in the β-phase. Whilst diffraction studies have not been able to distinguish between different disordered models, structure refinements of the β-phase have tended to produce better agreement between calculated and observed diffraction intensities when some disorder is introduced into the structure model than when the 'ideal' model is refined. However, even when the 'ideal' model is used in the refinement, the temperature factors lead to thermal ellipsoids that are signicantly elongated in directions normal to the {111} directions, consistent with the types of disorder proposed above.

Any model for disorder in β-cristobalite would predict the existence of structured diffuse scattering in a powder diffraction measurement. Wright and Leadbetter [18] predicted that a diffuse background would be generated from their model, but failed to measure it in an x-ray powder diffraction experiment. However, more recently Schmahl *et al* [1] found that there is a very distinct undulating background of diffuse scattering in neutron powder diffraction, which virtually vanishes on cooling into the α-phase. Diffraction experiments provide evidence of disorder, but it is difficult to tell the character of the disorder (static or dynamic) and whether well-defined unit-cell domains exist.

Strong planes of diffuse scattering have been observed in β-cristobalite in transmission electron microscopy (TEM) studies by Hua *et al* [6] and Withers *et al* [5]. The dependence of this diffuse scattering on wavevector is quite consistent with our RUM model [8].

Some degree of disorder is indicated by Raman and infrared spectroscopic studies. We have noted above that these studies do not lend support to specific domain models. All except two of the peaks that would be expected to disappear in the space group of the β-phase do so completely on heating above the transition. Both these peaks are very broad, in excess of 40 cm^{-1}, which is a typical signature of the existence of disorder, suggesting a fluctuation lifetime of less than 0.5 ps.

Finally, a recent inelastic neutron scattering measurement on a powdered sample showed that there is a large increase in the number of low-frequency modes on heating from the α-phase into the β-phase [8]. The existence of a significant number of low-frequency excitations is again a typical signature of the existence of disorder [8].

1.4. Aims of the present study

All the experimental work described above was carried out on powdered samples. This is a consequence of the fact that good quality single crystals of cristobalite are hard to acquire and tend to be rather mechanically unstable if cycled through the transition, and *large* single crystals, such as would be needed for neutron scattering studies, are simply not available. The restriction to work on powders limits the scope of experimental work that can be performed on cristobalite. Thus it is useful to turn to computational studies to provide new insights or supporting evidence for any model. There have been only two previous computational studies of cristobalite. Welberry *et al* [24] have reported some Monte Carlo simulations of the β-phase in support of their electron diffraction studies. More recently Tse and Klug [25] have performed a simulation of cristobalite at high pressure and of the phase transition at ambient pressure.

The purpose of the present study is to examine the nature of the disorder present in the β-phase of cristobalite using molecular dynamics simulations, with some supporting calculations performed in the α-phase. We have restricted ourselves here to the calculation of real-space quantities. At issue is the nature of the disorder in the β-phase, together with the intepretation of some of the experimental results obtained in this phase. Before we start to describe our work we first outline in some detail the RUM model as applied to cristobalite.

1.5. Rigid unit modes

We have recently proposed a new interpretation of the nature of the β-phase that is based on the concept of rigid unit modes [8, 20, 21, 22, 23]. RUMs are normal modes of vibration that can propagate without any distortion of the SiO_4 tetrahedra, at least within the small amplitude (harmonic) limit, and consequently RUMs can have relatively low frequencies. The possible existence of low-frequency modes in a framework silicate may be seen to arise by the description of the network in terms of a model potential of the form [8, 26]

$$V = \frac{1}{2}\sum_{(ij)} \alpha_{ij}(\Delta r_{ij})^2 + \frac{1}{2}\sum_{(ijk)} \beta_{ijk}(\Delta\theta_{ijk})^2 \qquad (1)$$

where α_{ij} and β_{ijk} are the intratetrahedral Si–O bond-stretching and O–Si–O bond-bending force constants respectively. In this model potential there are no intertetrahedral terms governing the Si–O–Si angle, although these forces will exist in reality. Strong intratetrahedral restoring forces and negligible intertetrahedral interactions lead to an approximation where the SiO_4 tetrahedra may be treated as rigid units, whose mutual orientations are nearly independent. The concept of RUMs arises naturally from this approximation—the RUM solutions to the corresponding phonon equations will have zero frequency [8, 21, 22, 23]. The actual existence of any RUM solutions follows from a subtle point of symmetry. In principle the existence of zero-frequency modes follows from a system having fewer independent geometrical constraints than degrees of freedom. For a framework structure consisting of linked tetrahedra there is at face value an exact balance between the numbers of geometrical constraints and degrees of freedom, so these are marginal cases having an expected zero number of RUM solutions. However, symmetry can cause some of the geometrical constraints to be linearly dependent. It turns out that in all crystalline frameworks the effect of symmetry is to allow a small but significant number of RUMs to be supported. The set of RUMs that may exist in the β- and α-phases of cristobalite have been previously determined [8, 22, 23] and are given in tables 1 and 2. From table 1 it can be seen that in the β-phase there are RUMs for whole planes of wavevectors in reciprocal space. The planes and lines observed in TEM [5, 6] all correspond to directions in which

Table 1. Rigid unit modes in β-cristobalite.

Wavevector	Rigid unit mode[a]
0, 0, 0 (Γ)	$T_{1u} + T_{2u}$ [b]
0, ξ, 0 (Δ)	$^2\Delta_3$
ξ, ξ, ξ (Λ)	$^2\Lambda_3 + \Lambda_2$
ξ, ξ, 0 (Σ)	Σ_2
$\frac{1}{2}, \frac{1}{2}, \frac{1}{2}$ (L)	$^2L_4 + L_2$
ξ, 1, ξ (S)	S_2
0, 1, 0 (X)	$^2X_4$
ξ, ξ, ζ (Θ)	$^2\Theta$

[a] The superscripts denote the degeneracy of the modes, and the subscripts refer to the symmetries of the modes.
[b] T_{1u} is an acoustic mode.

Table 2. Rigid unit modes in α-cristobalite. Note that there are many fewer RUMs than in β-cristobalite and that the ε-direction in α-cristobalite is parallel to the Σ-direction in β-cristobalite.

Wavevector	Rigid unit mode[a]
0, 0, 0 (Γ)	$A_2 + E + B_1$ [b]
ξ, ξ, 0 (ε)	$2\epsilon_2$
1/2, 1/2, 0 (M)	$^2M_2$

[a] The superscripts denote the degeneracy of the modes, and the subscripts refer to the symmetries of the modes.
[b] A_2 and E are acoustic modes.

RUMs are predicted (tables 1 and 2). The number of RUMs in the cubic β-phase is much greater than that in the tetragonal α-phase as the higher symmetry means that some of the constraints on the tetrahedra are no longer linearly independent [21]. The RUM model of β-cristobalite suggests a dynamically disordered structure, in which the disorder orginates from the action of a linear combination of RUMs of many different symmetries. The α-phase is relatively well-ordered as fewer RUMs are compatible with the lower symmetry.

Another piece of evidence for the existence of RUMs comes from the realization that the X_4 RUM at $k = (0, 1, 0)$ has been identified as providing the instability for the phase transition [8, 21, 22, 23], consistent with the analysis of Hatch and Ghose [9].

We may make a loose division between those RUM motions that are chiefly *rotational* and those that are chiefly *torsional* in character. Torsional motions are those which change the intertetrahedral Si–O–Si bond angle. Rotational motions are those which, at a fixed torsional angle, rotate the tetrahedra about the 'annulus'. In reality there is no restriction on a RUM in a real system to be purely rotational or torsional, but each will have some component of both sorts of motion. This point has been discussed in more detail elsewhere [20, 21].

2. Molecular dynamics simulation

The computer used for these simulations was the Cambridge University AMT DAP 610/32. The DAP (distributed array processor) is a massively parallel machine consisting of 4096 individual processing elements (PEs) laid out in a 64 × 64 square array. A major advantage of using the DAP for such simulations is the ability to map almost any lattice

onto the array. The long-vector method of indexing the 64×64 array [27] was used to simulate a cube of 16×16×16 with skew periodic boundary conditions, where each PE contains one unit cell. Another is the large sample size which may be simulated. The larger the sample size, the more representative of the bulk will the simulation become. This is particularly important when examining the nature of a system such as β-cristobalite. RUMs are present in planes in k-space (table 1) and a small sample size will sample very few wavevectors. Small scale simulations will detect fewer RUMs and, therefore, fewer modes of framework distortion. Domains are, therefore, far more likely to be observed in small scale simulations as fewer competing symmetries of the RUM fluctuations are sampled.

The program used for the simulation is based upon one written for the simulation of quartz by Tautz *et al* [28], and the phases of $MgSiO_3$ pervoskite [29]. The program is based upon a classical microcanonical NVE ensemble. The potential used in these simulations was that of the two-body Gilbert potential of Tsuneyuki *et al* [30]. Tsuneyuki *et al* deduced partial effective charges for q_i, of +2.4 for Si and −1.2 for O. The potential constants were developed on a quantum mechanical basis. This potential has been shown to give reasonably accurate parameters for the structure and lattice dynamics of α-quartz [25, 31] and has been applied to an MDS bulk study of the phases of quartz [32]. Its chief limitation appears to be a poor reproduction of the behaviour of α-quartz under pressure [25]. As this study is at ambient pressure, the potential of Tsuneyuki *et al* [30] is well suited to the study of disorder in β-cristobalite.

The time step chosen for the simulation was 2 fs. For the first cycle of the first run each of the atoms was given a random displacement. For the next 2000 steps (0.4 ps) the system was equilibrated by rescaling the individual velocities to maintain constant temperature in the ensemble. After this, the simulation was allowed to find its own unbounded equilibrium.

The program was set up to simulate α-cristobalite in its standard setting of $P4_12_12$ (No 92) of the *International Tables for Crystallography* [33] with 12 atoms per cell and cell parameters $a = 4.9694$ Å and $c = 6.9256$ Å. The initial atomic coordinates were taken from the results of the Rietveld refinements of Schmahl *et al* [1]. The temperature of the α-simulation was 200 °C. The Coulomb sum was evaluated using the Ewald method. The real space cut-off was 7 Å for both simulations. The reciprocal space cut-offs were 3.77 and 3.87 $Å^{-1}$ for the α- and β-simulations respectively.

The β-simulations were performed by mapping the 'ideal' β-cristobalite structure onto the $P4_12_12$ structure. To maintain the cubic nature of the phase, the cell parameters were chosen so that $\sqrt{2}a = \sqrt{2}b = c$. The relative orientations of the α and β lattices in the simulations were then the same and both α and β simulations involved 12 atoms/cell.

3. Single-phonon density of states

The phonon density of states, $g(\omega)$, represents the total number of phonon modes (or *states*) of a given frequency, ω, per unit volume and may be expressed as

$$g(\omega) = \sum_s \int \frac{d\boldsymbol{k}}{2\pi^3} \delta(\omega - \omega_s(\boldsymbol{k})) \tag{2}$$

where s is the label of a phonon dispersion branch propagating along the wavevector $\boldsymbol{k}$. The calculation of the density of states in MDS may be achieved by calculating the single-particle velocity self-correlation function, $C(t)$, over a period of several ps. This is expressed as

$$C(t) = \frac{\langle v(0).v(t)\rangle}{\langle v(0).v(0)\rangle} \tag{3}$$

where the brackets ⟨⟩ indicate an ensemble average.

Four independent correlation functions were calculated in each simulation so that they may be averaged to give some idea of the errors involved. The single-phonon density of states is the mass-weighted Fourier transform of this correlation function [34]. The calculated Fourier transform was weighted with the scattering lengths of Si and O so that the single-phonon density of states is what would be observed in an ideal neutron scattering experiment. The scattering lengths used for Si and O were 0.4149 and 0.5309 fm, respectively. The calculated densities of states for both phases are shown up to 40 THz in figure 3. Both densities of states were normalised to have an area of unity. The high frequency modes above 25 THz correspond to symmetric Si–O stretches, whilst the antisymmetric stretches lie between *ca.* 20 THz and 16.5 THz [35]. Si–O–Si intratetrahedral bending modes and torsional SiO_4 modes lie below 16.5 THz. At frequencies below about 1.5 THz there is a more rapid rise in the β-phase than the α-phase. This is discussed in more detail below.

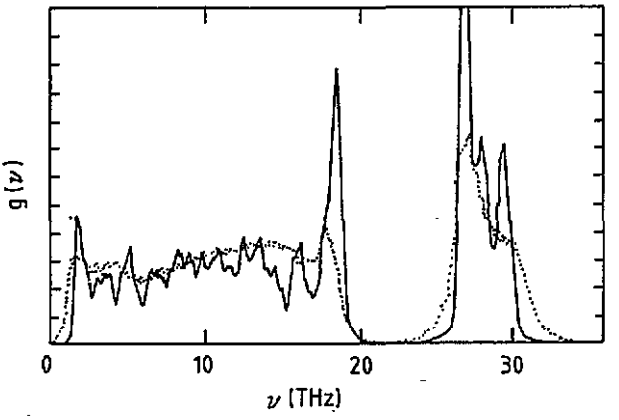

Figure 1. Results of the single-phonon density of states calculations from the α (solid lines) and β (dotted lines) simulations.

3.1. Inelastic neutron spectroscopy

In order to confirm our predictions of the existence of RUMs in cristobalite, we have performed some inelastic neutron scattering experiments on cristobalite. The sample was grown synthetically from a 99.999% SiO_2 glass by heating at 1500 °C for 48 h. The experiments were performed on the TFXA spectrometer at the ISIS spallation neutron source. The incident neutrons have a wide spread of energies. Two detector banks are present at 43° on either side of the specimen, where pyrolitic graphite (002) analyser crystals select only monochromatic neutrons which are scattered into the time-of-flight detectors. Higher-order neutrons are absorbed with a Be filter. The standard 'time-focusing' TFXA software was used to deduce the energy loss.

TFXA measures $S(|Q|, \nu)$ for a parabolic trajectory in $(\nu, |Q|^2)$, using a fixed analysing energy. Although this trajectory does not sample a true density of states, since the $|Q|$ averaging is not complete, the sampling will be reasonable for modes with frequencies only weakly dependent on wavevector. RUMs are very low-energy excitations and are therefore virtually independent of wavevector [22]. Therefore, the parabolic trajectory

gives a reasonably unbiased spectrum for the RUMs. The samples were packed in an Al foil folded into a slab several mm thick, and placed inside a heater containing two side heating elements shielded from the beam. The sample chamber was evacuated during the measurement. Temperature stability was better than ±7 °C. This was not critical to the experiment, as the RUM model predicts that the largest change in the inelastic spectrum will occur at T_{tr}. Measurements of the inelastic spectrum were performed at temperatures of 20 °C and 320 °C, well within the stability range of each phase. Each measurement took approximately 10 hours. Figure 3.1 shows the results of the experimental measurements for energies between 0–2.5 THz. As no background corrections were performed for this measurement, and the $|Q|$ sampling is not quite complete, it is not possible to determine the absolute number of states. However, figure 2 shows that there is a strong relative increase at low frequencies in $S(|Q|, \nu)$ (and, therefore, in the number of low-frequency modes) in β-cristobalite with respect to α-cristobalite. This is just what would be expected from the RUM model of the cristobalite framework: the bonding in the framework has not changed (the number of *raw* geometrical constraints is constant), but the symmetry has increased so that the number of *independent* geometrical constraints has been reduced. Consequently the number of RUMs is expected to increase.

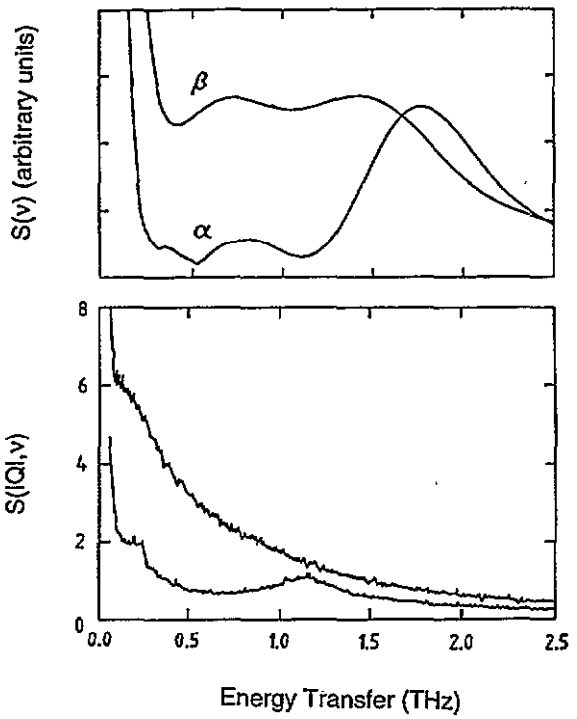

Figure 2. Top: calculated $S(\nu)$ from the MD simulation. Bottom: TFXA spectra of $S(|Q|, \nu)$ of cristobalite for the low-frequency regime. The data from the α-phase are on the lower curve.

As the averaging of the trajectory measured by TFXA is not easily calculated in the DAP we also display in figure 2 the calculated function $S(\nu)$ from the MD simulation as a simple comparison in the low-frequency region. This is related to $g(\nu)$ simply as $S(\nu) = g(\nu)/\nu^2$, ignoring such effects as multiphonon and multiple scattering. As the two functions are differently weighted only a qualitative comparison is possible. The chief similarity between

the measured and calculated function is that in the β-phase there is more of a continuum of low-frequency modes than in the α-phase, where a distinct maximum is found. There is a systematic difference between the maximum seen in the α-cristobalite in the measured and calculated spectra, probably due to the finite sample simulation size and to small errors in the potential. However, in general the results of the MDS calculations and measured inelastic spectra are in agreement about the relative number of modes at low-frequencies.

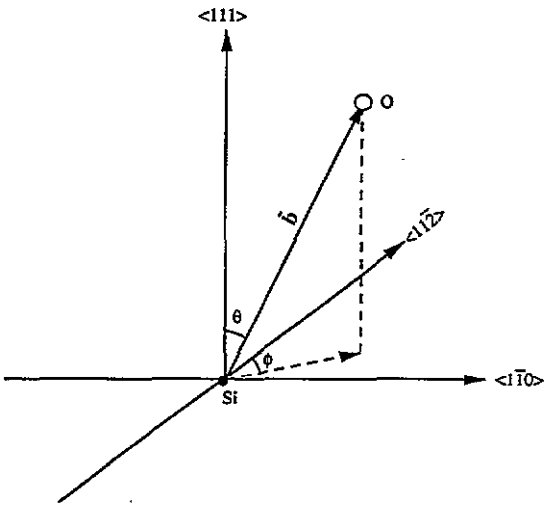

Figure 3. Relationship between the Si–O bond vector b, the crystallographic axes $\langle 111 \rangle$, $\langle 1\bar{1}0 \rangle$ and $\langle 11\bar{2} \rangle$. The ideal Si–O orientation is along the $\langle 111 \rangle$ axis. θ is the torsional angle between $\langle 111 \rangle$ and b. ϕ is the azimuthal angle arbitrarily defined with respect to the $\langle 11\bar{2} \rangle$ axis.

4. Orientation of the Si–O bonds in β-cristobalite

4.1. Characteristics of the ensemble

The bond orientation is described with the use of the spherical polar coordinates θ and ϕ. Figure 3 displays the relationship between the Si–O bond vector b, the crystallographic axes and the angles θ and ϕ. θ (the torsional angle) is defined as the deviation away from the 'ideal' $\langle 111 \rangle$ Si–O bond vector. The angle ϕ (the azimuthal angle of rotation) is defined as the projection of this vector down into the orthogonal $\langle 11\bar{2} \rangle$–$\langle 1\bar{1}0 \rangle$ plane; i.e. at a fixed θ, ϕ defines the position around the annulus. This examination of the orientational distribution of the Si–O bonds was performed to search for signatures of RUMs in the local motions, and to assess whether or not domains were formed by their action.

The possibility exists that the Si–O bond vectors precess by making discrete jumps of fractions of 360° about the 'annulus'. We therefore examined the correlations of the motions of the Si–O vectors around the 'annulus' with an orientational correlation function (OCF), $C(\phi(t))$, defined as

$$C(\phi(t)) = \frac{\langle \cos\phi(t).\cos\phi(0) \rangle}{\langle \cos\phi(0).\cos\phi(0) \rangle}. \tag{4}$$

The corresponding OCFs $C(2\phi(t))$, $C(3\phi(t))$ and $C(6\phi(t))$ were also calculated in order to examine the dynamics of rotation, and to see whether there were any tendencies to rotate in

jumps of 360°, 180°, 120° or 60°, respectively. These are shown in figure 4. The results are the average of four time-series calculations. It is obvious that the higher order OCFs rapidly decay to zero, indicating that there is little correlation in time between ϕ angles 180°, 120° or 60° apart. The higher order correlation functions decay progressively more rapidly.

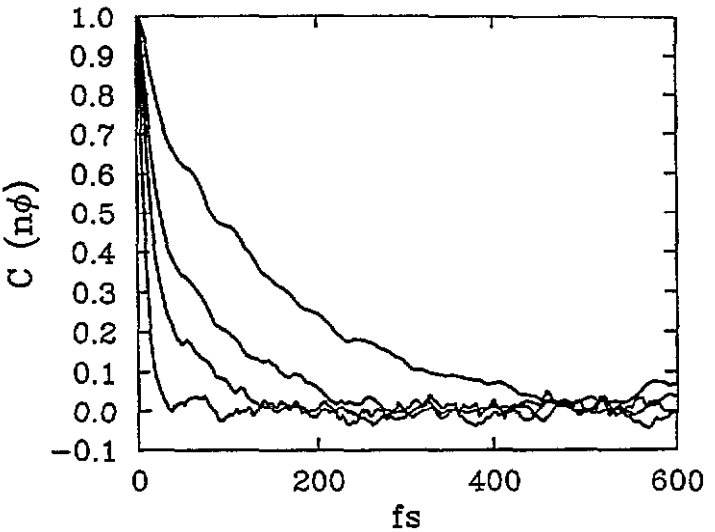

Figure 4. Orientational correlation functions of the β simulation. In order of increasing decay rate they are $C(\phi(t))$, $C(2\phi(t))$, $C(3\phi(t))$ and $C(6\phi(t))$. The results are the average of four independent time-series.

The calculated θ angle distribution, $p(\theta)$, together with the function $p(\theta)/\sin(\theta)$, is shown in figure 5. The function $p(\theta)/\sin(\theta)$ shows a broad peak extending quite some distance from the central $\theta = 0°$ peak, clearly showing that bond angle disorder is present in the system. The calculation was performed by averaging the instantaneous orientation of one Si–O vector from each of the 4096 PEs at four different time steps, each 100 time steps apart. $p(\theta)$ is broad and slightly asymmetric with its maximum at *ca.* 16°, corresponding to an average value of the Si–O–Si angle ($180° - 2\theta$) of *ca.* 148°. $p(\theta)$ is interesting in the light of comparison to the experimentally determined function $V(\alpha)$ of silica glass in the classic paper of Mozzi and Warren [36]. This experimentally measured distribution is also very broad, although it is likely in the case of a glass that the orientations of any one Si–O bond have much greater constraints placed upon them than in the crystal, so that the distribution is more static in character. The comment of Mozzi and Warren [36] that the measured broad angular distribution of glass is a characteristic distinguishing between amorphous and crystalline silica would appear to have been made with regard to the α-phases, where the relatively static nature gives a well defined bond angle.

We also define a cumulative bond angle distribution, $P(\theta)$, which is related to $p(\theta)$ by

$$P(\theta) = \int_0^\theta p(\theta')\,\mathrm{d}\theta' \tag{5}$$

and is shown in figure 6. This reveals that one quarter of the bonds lie below 12°, a half below 16° and three quarters below 21.5°.

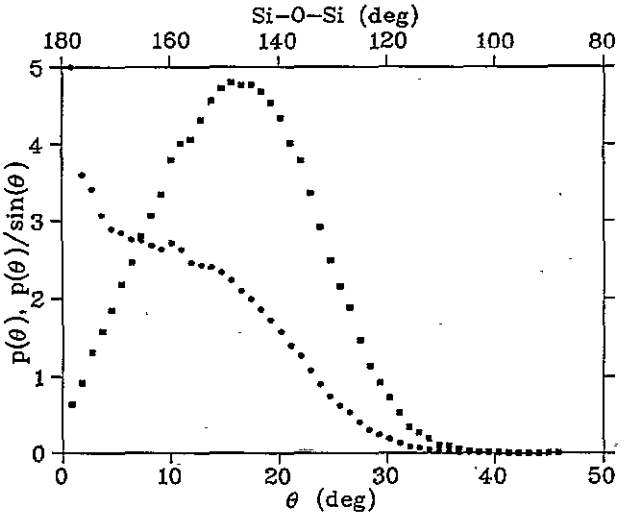

Figure 5. θ bond angle distributions, $p(\theta)$ and $p(\theta)/\sin(\theta)$, defining the deviation away from the 'ideal' orientation. $p(\theta)/\sin(\theta)$ shows the presence of a very broad peak at $\theta \neq 0°$, indicative of bond angle disorder. $p(\theta)$ shows a distribution with great similarity to that derived by Mozzi and Warren [36]. The distribution is an average of one Si–O vector from each of 4096 PES, and averaged from 4 time steps, each 100 time steps apart.

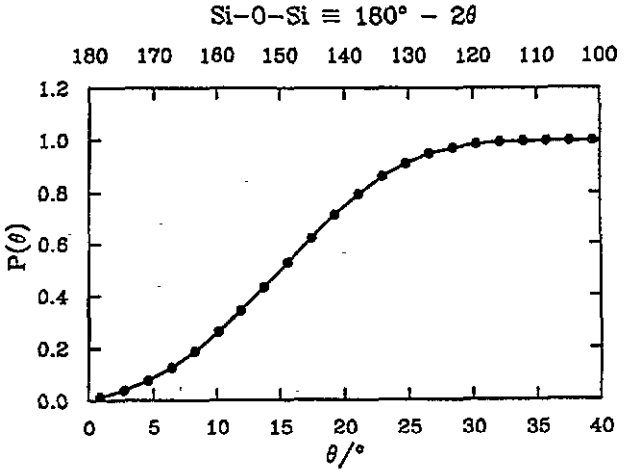

Figure 6. Cumulative distribution function ($P(\theta)$) of the θ angle.

Figure 7 shows a map of θ–ϕ of the same Si–O bond vector shown in figures 5 and 6. The broad distribution of Si–O bond vectors in θ is obvious, as is the fact that the distribution in ϕ is nearly isotropic. Any ϕ-dependence is extremely weak and there are no positions about the 'annulus' that are well-defined with respect to the crystal axes. This is incompatible with any domain models of the β-phase, all of which are based on clusters of Si–O bond orientations forming at special equivalent points within the space group $Fd\bar{3}m$.

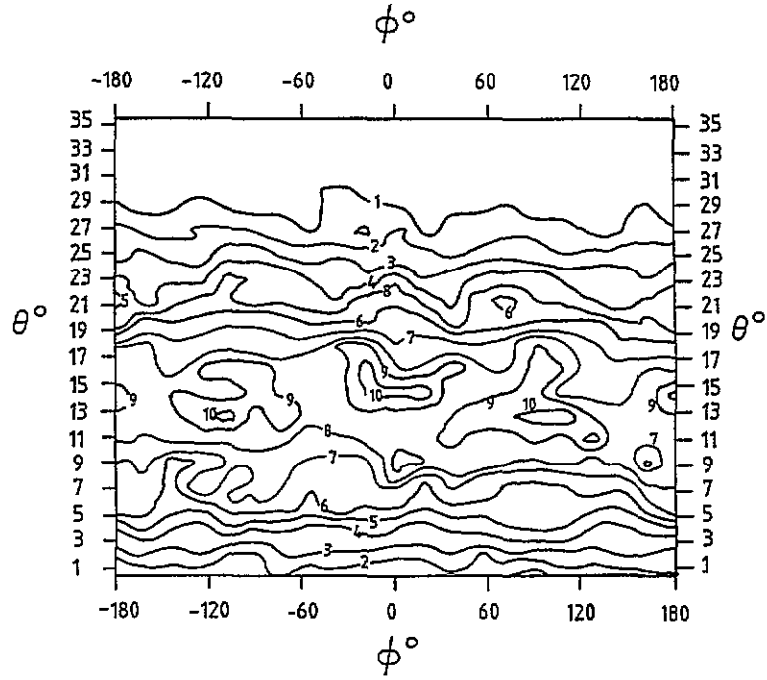

Figure 7. θ–ϕ map of bond vector distributions in the ensemble. The contours were arbitrarily scaled from zero to ten (maximum occupation). The distribution is an average of one Si–O vector from each of 4096 PEs, and averaged from 4 time steps, each 100 time steps apart. There is at best, an extremely weak ϕ-dependence which can just be discerned, and no evidence of domains.

4.2. Characteristics of single Si–O vectors

Figure 8 shows the motion of a single bond vector from one PE of the simulation. This shows that the bond vectors display a large degree of dynamic disorder. It must be stressed that these rotations are not uncommon in the simulation; this particular bond vector has been chosen out of many we have examined to illustrate the case. Over an equivalent time scale many bonds will not flip even once about the 'annulus', but all show some dynamic fluctuation. The sudden drop in the lower diagram, at *ca.* 1.9 ps, is due to the atom moving right around the 'annulus' and leaving the upper bound of the precession angle, at $\phi = 180°$, and re-entering at the lower bound at $\phi = -180°$: the apparently extreme discontinuity in the graph actually corresponds to a fairly continuous rotation. The complete rotation about the 'annulus' occurs in under 0.4 ps. The bond is not continuously spinning about the 'annulus', but spends the majority of its time making rather smaller fluctuations in orientation. The inclination angle, θ, is also disordered. In fact, although the angular range is smaller in magnitude, the θ fluctuations are even more impressive, as the range 0–28° corresponds to fluctuations in Si–O–Si bond angle ($180° - 2\theta$) of 180–124°. There appears to be some correlation between the two angles, for instance where ϕ makes fairly rapid changes (e.g. *ca.* 0.5 ps, *ca.* 1 ps, *ca.* 1.4 ps and *ca.* 2.05 ps) there appear to be corresponding changes in θ. However, at least for the last three examples, this may be exacerbated as θ falls to very small angles, making the definition of ϕ rather difficult. The spread of θ in the $p(\theta)$ of figure 5 is, therefore, not due to varying static inclinations of individual bonds. Instead both orientational variables are fluctuating quantities.

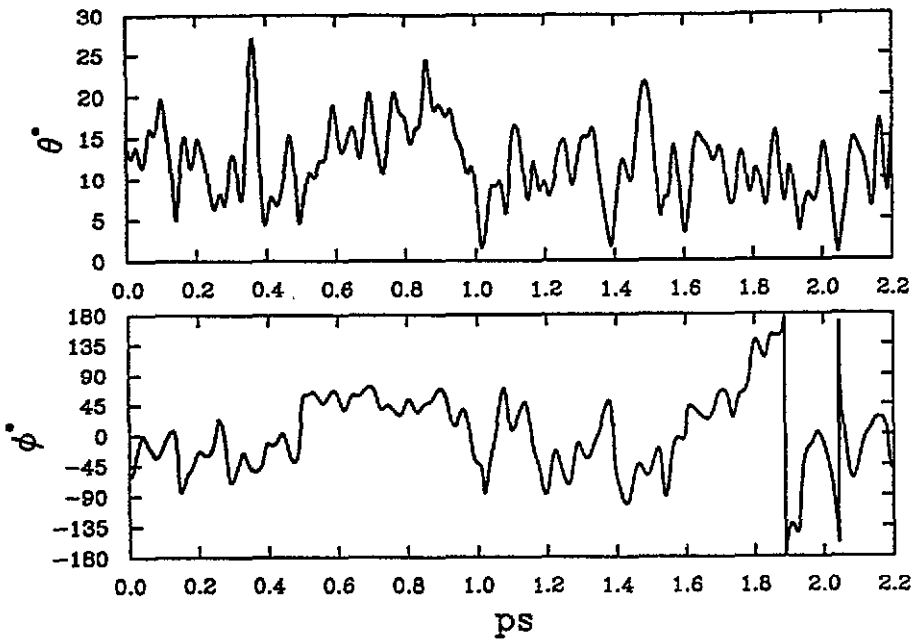

Figure 8. An example of a single bond undergoing dynamic reorientation in β-cristobalite.

5. Pair distribution functions

The *pair distribution function*, $g(r)$ is a common measure of order in a structure. It is often employed in the description of amorphous materials. In the case of cristobalite, we are interested in the pair distribution functions as a measure of the existence of disorder induced in the lattice by low-frequency modes. It is possible to calculate $g(r)$ directly in a simulation. $g(r)$ tends to show quite sharp peaks at low r where local chemical considerations give rise to short-range order, such as rigid SiO_4 tetrahedra. As $r \rightarrow \infty$, $g(r) \rightarrow 1$ as inter-particle effects vanish in this limit and the number of pairs tends to the average number expected from the mean density if there were no interparticle influence present.

In addition it is possible to extract the partial pair distribution function, by counting distances between certain pairs of atoms only. $g_{Si\text{-}Si}(r)$, $g_{Si\text{-}O}(r)$ and $g_{O\text{-}O}(r)$ are shown displayed in figures 9, 10 and 11 respectively. Even in a perfectly ordered, ideal crystal $g(r) \rightarrow 1$ as $r \rightarrow \infty$, so comparison of degrees of order becomes more difficult at very high r. However, these figures demonstrate that the α phase is more ordered on nearly all length scales beyond the level of the tetrahedron, reflecting a more constricted O distribution, as there are fewer RUMs present in the α-form. In both phases $g_{Si\text{-}Si}(r)$ has much greater correlations at higher r than either $g_{O\text{-}O}(r)$ or $g_{Si\text{-}O}(r)$. These latter functions decay much more quickly. This reveals that the Si sites (the centres of gravity of the tetrahedra) are less affected than the tetrahedral orientation (defined by the O positions). However, comparing $g_{Si\text{-}Si}(r)$ between the two phases reveals that the higher RUM amplitude does cause a greater smearing of the centres of gravity in the β phase. Both rotational and torsional RUM motion will tend to average $g_{O\text{-}O}(r)$ and $g_{Si\text{-}O}(r)$, whereas only torsional motion will affect $g_{Si\text{-}Si}(r)$.

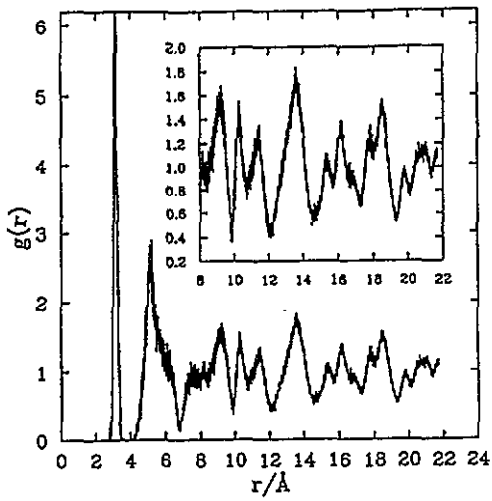

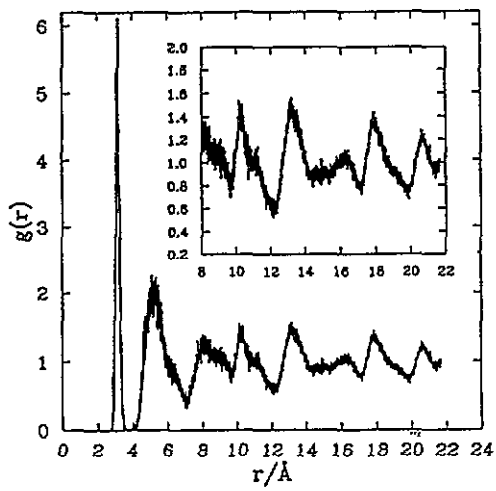

Figure 9. The partial pair distribution function of $g_{Si\text{-}Si}(r)$ for α (top) and β (bottom) simulations.

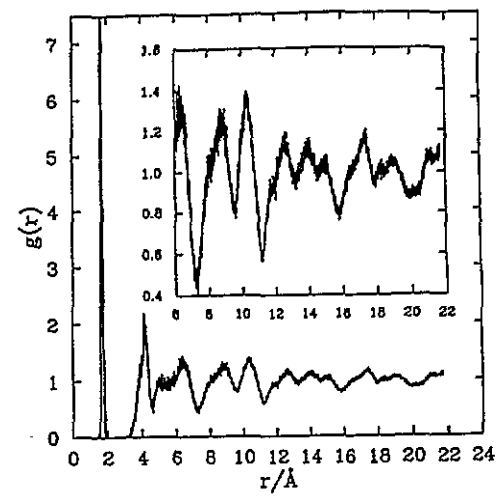

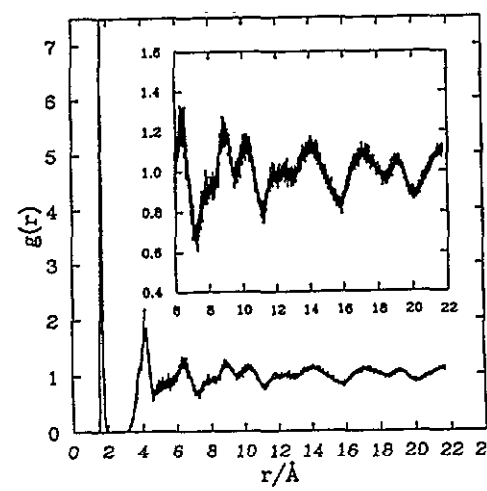

Figure 10. The partial pair distribution function of $g_{Si\text{-}O}(r)$ for α (top) and β (bottom) simulations.

6. Structure factors of β-cristobalite

The structure factor $S(Q)$ represents what would ideally be measured in a neutron diffraction experiment. A previous neutron powder diffraction measurement has been made of cristobalite using the instrument HRPD at ISIS [1]. A large undulating background was seen in the spectrum of the β-phase which was not present in the spectrum of the α-phase. To check the possibility that the RUM-induced disorder was the origin of this effect we calculated $S(Q)$ for β-cristobalite. For comparison we calculated the partial structure factors from each of the partial pair distribution functions in order to see which of these gave the largest contribution. The partial structure factor, $S_p(Q)$, is related to the (partial)

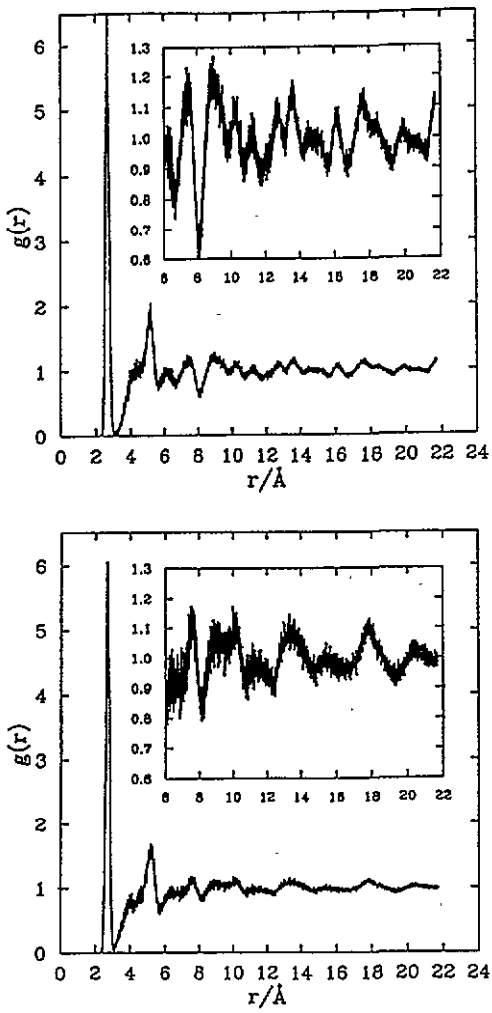

Figure 11. The partial pair distribution function of $g_{O\text{-}O}(r)$ for α (top) and β (bottom) simulations.

pair distribution function $g_p(r)$ by the Fourier transform

$$S_p(Q) = 1 + \rho \int_0^\infty (g_p(r) - 1) \exp i(Q \cdot r)\, dr \tag{6}$$

where ρ is the mean number density of particles in the lattice. This can be simplified to a function of the form

$$S_p(Q) = 1 + \rho \int_0^\infty (g_p(r) - 1) \frac{\sin(Qr)}{Qr} 4\pi r^2\, dr \tag{7}$$

if the assumption is made that the distribution is isotropic [37].

The structure factors from each of the partial pair distribution functions of β-cristobalite, $g_{Si\text{-}Si}(r)$, $g_{Si\text{-}O}(r)$, $g_{O\text{-}O}(r)$, were calculated using equation (7). These are displayed in figure 12, along with the full structure factors of β-cristobalite, in the region of 4–32 $Å^{-1}$. In these calculations, the Fourier transform was weighted by the neutron scattering lengths

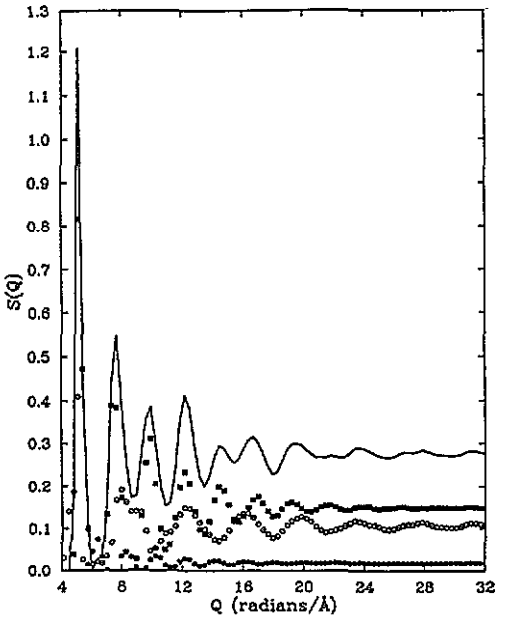

Figure 12. Calculated structure factors of cristobalite (solid line), formed from the partial structure factors from Si–Si interactions (closed circles), Si–O interactions (open circles) and O–O interactions (closed squares).

given in section 3. The total structure factor was then calculated by weighting each of the component structure factors by both the neutron scattering lengths and the proportion they contribute to the total. As Si is one third, and O two thirds of the total number of atoms per unit cell, the proportions (f) are 1/9, 4/9 and 4/9, respectively. The total $S(Q)$ is then defined as

$$S(Q) = 1 + \rho \sum_{\text{partials}}^{\text{all}} f \int_0^\infty (g_p(r) - 1) \frac{\sin(Qr)}{Qr} 4\pi r^2 \, dr. \tag{8}$$

The small weighting of 1/9 on $S(Q)_{\text{Si–Si}}$ means that its contribution to the total $S(Q)$ is so small that it barely affects the end result (see figure 12). This weighting infers that the humps are chiefly generated by the dynamic O disorder in the lattice. This fits well with the fact that all RUMs produce O motion, whereas only torsional RUMs move the centre-of-mass of the SiO_4 tetrahedra. The weighting reduces the significance of such motion still further.

Schmahl *et al* [1] measured the neutron powder diffraction spectra of β-cristobalite. No background corrections were made for these measurements and the measured spectra contain scattering from both the can and the furnace. It is, therefore, not an absolute measurement. However, three broad maxima are seen in the background as diffuse scattering at 58 000, 36 000 and 25 000 μs. These were not present in the α-phase and are, therefore, related to the dynamic disorder. The conversion factor for time-of-flight to d-spacing for HRPD is 2.07×10^{-5} μs Å^{-1}. In Q, these maxima are at 5.23, 8.43 and 12.14 Å^{-1}.

In the middle range, the total structure factor shows a series of peaks. The positions of the centres of the first four of these peaks were measured, and were found to be at 5.20, 7.60 and 9.83 and 12.16 Å^{-1}. In general, the features in the measured spectrum are broader than those in the calculated structure factor. The broad hump observed centered at *ca.* 36 000 μs

appears to correspond to two maxima in the structure factor calculations, but otherwise the agreement between experiment and calculation is good.

We have demonstrated that the $S(Q)$ calculated from the simulation of the β-phase correlates well to that seen in the neutron powder diffraction study. This implies that the nature of the disorder in the β simulation is characteristic of that in the real system, i.e. that the disorder is dynamic, RUM-induced, and that domains are not required to explain the structured diffuse scattering.

7. Previous simulations

The only previous large scale simulation of cristobalite concentrating on the nature of the β-phase is the MC study by Welberry *et al* [24]. The MC simulation was based upon interactions between the atoms using a force constant model. The values of this force constant model had been calculated from fitting to the Raman spectrum of α-cristobalite as measured by Bates [19]. They found that this model produced a deviation from the 'ideal' O position an order of magnitude less than that required for the static occupation of the 96(h) sites of the Wright and Leadbetter model [18]. Unlike this simulation, their subsequent simulations were placed under a number of strong constraints on the structure and force constant values.

One model removed all direct Si–Si interactions and added an Si–O–Si bond bending term to the force constant model of the form

$$E_{\mathrm{Si-O-Si}} = K(\theta - 147)^2$$

with K chosen to force the Si–O–Si to take up values of 147°, within a standard deviation of 0.5°. This model produced an essentially uniform distribution of O atoms around an annulus, defined about the 'ideal' position. Their most sophisticated model involved, amongst other constraints, the addition of a second nearest neighbour O–O interaction and a term dependent on the O–Si–O–Si dihedral angle. Their reason behind this was to try to induce ordering, but they could find no potential which could do so to any significant degree.

To calculate how the scattering from a system with partial ordering would appear, they placed a different constraint on their system. Two of their models took the O positions of this first model and moved them 20% and 40%, respectively, towards their nearest 96(h) position. The purpose behind this forcing of the simulation was to calculate the diffuse scattering from such geometries. Their conclusions, based upon the calculated diffraction patterns, was that increased ordering towards the 96(h) sites was a worse description of the β phase than the 'ideal' structure! Their best description came from the model constrained to the 147° tilt from the 'ideal' orientation—the mean value of the broad distribution obtained from our unconstrained simulation.

8. Conclusions

The conclusions from the previous MC and this MD simulation regarding the nature of the β-phase are very similar. There is no evidence of any preference for crystallographically distinct domains. Because of the lack of any significant ϕ-preference in both studies, both the model of Hatch and Ghose [9] and a dynamic interpretation of the model of Wright and Leadbetter [18] would appear to be ruled out.

The results of this MD simulation paint a very clear picture of β-cristobalite as a dynamically disordered system, in which the $Fd\bar{3}m$ symmetry is preserved. It is a summation of RUMs of many different symmetries that generates the dynamic disorder, and for this reason domain models appear to be a poor description of β-cristobalite. The dynamic

disorder observed in the simulations has been shown to be consistent with the modulations in the background of the neutron powder diffraction spectra of Schmahl *et al* [1]. The original disordered annulus model of Nieuwenkamp [17] is closest to the simulation results, although it is obvious that if the term 'annulus' is to be used, it should not be thought of as a fixed radius annulus, but rather as a very broad probability distribution, as is shown by figure 5. The dynamic disorder has been shown to mainly affect the O atoms (see section 5) and to be present to a much larger extent in the β phase than the α phase, which is consistent with predictions made from the RUM description of the system.

References

[1] Schmahl W W, Swainson I P, Dove M T and Graeme-Barber A 1992 *Z. Kristallogr.* **201** 125
[2] Swainson I P and Dove M T 1994 *Phys. Chem. Minerals* submitted
[3] Spearing D R, Farnan I and Stebbins J F 1992 *Phys. Chem. Minerals* **19** 307
[4] Phillips B L, Thompson J G, Xiao Y and Kirkpatrick R J 1993 *Phys. Chem. Minerals* **20** 341
[5] Withers R L, Thompson J G and Welberry T R 1989 *Phys. Chem. Minerals* **16** 517
[6] Hua G L, Welberry T R, Withers R L and Thompson J G 1988 *J. Appl. Crystallogr.* **21** 458
[7] Swainson I P and Dove M T 1994 *Phys. Chem. Minerals* at press
[8] Swainson I P and Dove M T 1993 *Phys. Rev. Lett.* **71** 193
[9] Hatch D M and Ghose S 1991 *Phys. Chem. Minerals* 17 554
[10] Liu F, Garolfalini S H, King-Smith R D and Vanderbilt D 1993 *Phys. Rev. Lett.* **70** 2750
[11] Swainson I P and Dove M T 1993 *Phys. Rev. Lett.* **71** 3610
[12] de Biasi R S and Simões A 1987 *J. Phys. C: Solid State Phys.* **20** 5573
[13] de Biasi R S and Simões A 1989 *J. Phys.: Condens. Matter* **1** 5915
[14] Hatch D M, Ghose S and Bjorkstam J L 1994 *Phys. Chem. Minerals* **21** 67
[15] Wyckoff R W G 1925 *Am. J. Sci.* **9** 448
[16] Wyckoff R W G 1925 *Z. Kristallogr.* **62** 189
[17] Nieuwenkamp W 1937 *Z. Kristallogr.* **96** 454
[18] Wright A F and Leadbetter A J 1975 *Phil. Mag.* **31** 1391
[19] Bates J B 1972 *J. Chem. Phys.* **57** 4042
[20] Vallade M, Berge B and Dolino G 1992 *J. Physique I* 2 1482
[21] Dove M T, Giddy A P and Heine V 1992 *Ferroelectrics* **136** 33
[22] Dove M T, Giddy A P and Heine V 1992 *Trans. Am. Crystallogr. Assoc.* **27** 697
[23] Giddy A P, Dove M T, Pawley G S and Heine V 1993 *Acta. Crystallogr.* **A49** 697
[24] Welberry T R, Hua G L and Withers R L 1989 *J. Appl. Crystallogr.* **22** 87
[25] Tse J S and Klug D D 1991 *J. Chem. Phys.* **95** 9176
[26] Thorpe M F 1983 *J. Non-Cryst. Solids* **57** 355
[27] Pawley G S and Thomas G W 1982 *J. Comput. Phys.* **47** 165
[28] Tautz F S, Heine V, Dove M T and Chen X 1991 *Phys. Chem. Minerals* **18** 326
[29] Winkler B and Dove M T 1992 *Phys. Chem. Minerals* **18** 407
[30] Tsuneyuki S, Tsukuda M, Aoki H and Matsui Y 1988 *Phys. Rev. Lett.* **61** 869
[31] Cowley E R and Gross J 1991 *J. Chem. Phys.* **95** 8357
[32] Tsuneyuki S, Aoki H and Tsukuda M 1990 *Phys. Rev. Lett.* **64** 776
[33] Hahn T (ed) *International Tables for Crystallography* 1984 (Dordrecht: Reidel)
[34] Dove M T 1993 *Introduction to Lattice Dynamics* (Cambridge: Cambridge University Press) ch 12 appendix F
[35] Kramer G J, Farragher N P, van Beest B W H and van Santen R A 1990 *Phys. Rev. Lett* **64** 1955
[36] Mozzi R L and Warren B E 1969 *J. Appl. Crystallogr.* 2 164
[37] Cusack N E 1988 *The Physics of Structurally Disordered Matter: An Introduction* (Bristol: Adam Hilger)